THE NATURE OF THE LOW ENERGY ISOVECTOR DIPOLE EXCITATIONS IN NUCLEI

A Senior Scholars Thesis

by

EMILIAN NICA

Submitted to the Office of Undergraduate Research
Texas A&M University
in partial fulfillment of the requirements for the designation as

UNDERGRADUATE RESEARCH SCHOLAR

April 2009

Major: Physics

THE NATURE OF THE LOW ENERGY ISOVECTOR DIPOLE EXCITATIONS IN NUCLEI

A Senior Scholars Thesis

by

EMILIAN NICA

Submitted to the Office of Undergraduate Research
Texas A&M University
in partial fulfillment of the requirements for the designation as

UNDERGRADUATE RESEARCH SCHOLAR

Approved by:

Research Advisor: Shalom Shlomo
Associate Dean for Undergraduate Research: Robert C. Webb

April 2009

Major: Physics

ABSTRACT

The Nature of the Low Energy Isovector Dipole Excitations in Nuclei.
(April 2009)

Emilian Nica
Department of Physics
Texas A&M University

Research Advisor: Dr. Shalom Shlomo
Cyclotron Institute, Texas A&M University

Calculations of the nuclear response function for the Isovector Giant Dipole Resonance (IVGDR) have been carried out in the past using the discretized Hartree-Fock Random Phase Approximation (HF-DRPA). In many cases they contained violations of self-consistency and a large smearing parameter. To avoid any sources of error we carried out a self-consistent HF-Continuum RPA (HF-CRPA) to determine the IVGDR response function in ^{60}Ca, ^{28}O and ^{80}Zr. We have also examined the free p-h response in the continuum. In addition, we determined resonance energies through the phase shift method for ^{60}Ca and ^{28}O. The main goal of our research was to establish if the low-lying peaks in the response function were due to resonance or particle threshold effects. We have shown that in some cases the enhancements in the response function at low energies are due to threshold effects. We emphasize that in a discretized HF-RPA these peaks are spurious and are due to the discretization of the single-particle continuum.

ACKNOWLEDGMENTS

I would like to thank my advisor, Dr. Shalom Shlomo, for his guidance in research and help in the preparation of this thesis.

I want to acknowledge the support I received from my parents throughout this period.

I also want to thank the Undergraduate Research Scholar Program for providing an opportunity to undertake research.

NOMENCLATURE

HF	Hartree-Fock
DRPA	Random Phase Approximation with discretized continuum
CRPA	Random Phase Approximation with proper treatment of the continuum
IVGDR	Isovector Giant Dipole Resonance

TABLE OF CONTENTS

Page

ABSTRACT iii

ACKNOWLEDGMENTS iv

NOMENCLATURE v

TABLE OF CONTENTS vi

LIST OF FIGURES viii

CHAPTER

I INTRODUCTION 1

II FORMALISM 6

Hartree-Fock equations 6
Green's function approach to the linear response function 8
Discretized vs. continuum treatment 10
Phase shift calculations 12

III RESULTS 14

HF-CRPA results 14
Free response with a discretized continuum 21
Phase shift results 26

IV CONCLUSION 31

REFERENCES 33

Page

APPENDIX 34

CONTACT INFORMATION 39

LIST OF FIGURES

Page

Fig. 1. Isovector Dipole Continuum HF-CRPA for ^{60}Ca with smearing Γ/2=0.4 MeV and a maximum radius of 12 fm. 17

Fig. 2. Isovector Dipole Continuum HF-CRPA for ^{28}O with smearing Γ/2=0.4 MeV and a maximum radius of 12 fm. 17

Fig. 3. Isovector Dipole Continuum HF-CRPA for ^{80}Zr with smearing Γ/2=0.4 MeV and a maximum radius of 12 fm... 18

Fig. 4. Isovector Dipole Continuum HF-CRPA Free Response for ^{60}Ca with smearing Γ/2=0.4 MeV and a maximum radius of 12 fm 20

Fig. 5. Isovector Dipole Continuum HF-CRPA Free response for ^{28}O with smearing Γ/2=0.4 MeV and a maximum radius of 12 fm 20

Fig. 6. Isovector Dipole Continuum HF-CRPA Free response for ^{80}Zr with smearing Γ/2=0.4 MeV and a maximum radius of 12 fm 21

Fig. 7. Isovector Dipole Discretized HF for ^{60}Ca with a box size of 150 fm..... 23

Fig. 8. Isovector Dipole Discretized HF for ^{28}O with a box size of 150 fm. 25

Fig. 9. Isovector Dipole Discretized HF for ^{60}Ca with a box size of 12 fm..... 25

Fig. 10. Single-Particle Level Density for ^{60}Ca, for L=4 28

Fig. 11. Single-Particle Level Density for ^{28}O, for L=3..... 30

CHAPTER I

INTRODUCTION

The present thesis is concerned with the study of the possibility of low-lying resonances for the case of the Isovector Giant Dipole Resonance (IVGDR) in the neutron-rich nuclei ^{60}Ca and ^{28}O. In addition, we also study the IVGDR in the symmetric ^{80}Zr nucleus.

The IVGDR is a type of nuclear collective mode. G.C. Baldwin and G.S. Kleiber [1] discovered it experimentally in 1947 by observing a strong enhancement in the absorption cross-section of photons in heavy nuclei. Historically, there have been two distinct approaches to describe this collective phenomenon namely, the macroscopic Liquid Drop Model (LDM) and the microscopic Quantum Mechanics description. The Liquid Drop Model uses classical hydrodynamics to describe the nucleus through the use of proton and neutron liquid densities. In the case of the IVGDR, an incident electromagnetic wave displaces the proton liquid from its equilibrium position. The nuclear interactions provide a restoring force resulting in out of phase oscillations of the proton liquid against the neutron liquid. More precisely, the restoring force is attributed to the symmetry term in the Weizacker semi-empirical mass formula. The change in the symmetry energy can be expressed as a function of the changes in the positions of the

---

This thesis follows the style of Physical Review C.

two liquids. This in turn can be used to express the restoring force. The result is a wave equation for the proton density, from which one can extract the resonant frequency. We note that in the Liquid Drop Model for the IVGDR introduced by Goldhaber and Teller [2] the neutron liquid is oscillating against the proton liquid, whereas in Steinwedel and Jensen [3] model the IVGDR is described as a rearrangement of the neutron and proton liquids within a fixed nuclear volume.

In the microscopic model, the giant dipole resonance is seen as a transition between two nuclear states. In the dipole approximation, this requires a difference of angular momentum L=1 between the states. The participation of both neutrons and protons in the isovector excitations also necessitates a difference of isospin number T=1 between the initial and final state. The nuclear states are eigenstates of the many-body Hamiltonian with two-body nuclear interactions. In the mean-field approximation, the antisymmetric nuclear states are constructed as Slater determinants from single-particle wave functions. By applying the principle of variation to the expectation value for the binding energy of the ground state of the system, described as a Slater determinant, while constraining the single-particle states to be orthonormal, one can obtain the Hartree-Fock (HF) equations [4]. Each single-particle state is found to be an eigenstate for a mean-field potential which is formally identical for each single-particle state and dependent on all states. As such, the nucleons are seen as moving independently in the mean field [4]. Because of the dependence of the mean field on all single-particle states, the Hartree-Fock equations are solved iteratively. From an initial set of single-particle wave functions, chosen to

ensure convergence, one finds a mean-field that is in turn used to determine a new set of single-particle wave functions. The process is repeated until the eigenvalues (energies) of the single particle states converge. Because of its iterative nature this method is also termed self-consistent [4]. The HF equations are thus used to determine single-particle states and energies.

For dipole transitions, the nuclear excited states are described as a coherent superposition of particle-hole excitations. A particle-hole state is formed by exciting one particle in an unoccupied single-particle state, differing by one unit of angular momentum from the initial single-particle state. We use the nuclear states allowed under the dipole transition to calculate the response function. The states with large transition probabilities will correspond to resonance energies for the IVGDR. The spectrum of the collective nuclear states can be well described within the Random Phase Approximation (RPA) approach, which is used to facilitate the many-body calculations.

We focus on microscopic calculations involving a self-consistent Hartree-Fock mean field Random Phase Approximation (HF-RPA) scheme. The problem under study arises from the treatment of the continuum. It is common in the literature to carry out HF-RPA calculations by discretizing the continuum single-particle states (HF-DRPA). As such, the discretized continuum states are also bound states. Under this treatment, single-particle dipole transitions to the continuum will appear as sharp peaks in the free particle-hole response. It is also customary to undertake HF-DRPA calculations with

violations of self-consistency and large smearing parameters. Under these conditions, the low-lying enhancements in the response function have been interpreted as resonant states.

In a HF Continuum RPA (HF-CRPA) the particles excited into the continuum are free to decay. The widths of these transitions in the free p-h response are properly accounted for in this approach. As such, this method allows for a more accurate determination of resonance energies.

To test whether the low-lying enhancements in the RPA responses under discretized calculations alluded to above are indeed resonances, we carry out HF-CRPA calculations for the three nuclei under study. We compare the Free responses for the HF-CRPA with the Free responses obtained with a discretized continuum. As a check on our results, we also determine the derivatives of the scattering phase shifts with respect to energy.

In Chapter II we discuss the HF-CRPA theory in detail. The derivation of the HF equations and a discussion of the RPA are given. We present the RPA Green's function formalism as it pertains to our calculations along with a method developed by Dr. Shalom Shlomo, used to properly account for continuum excitations. A brief description of the method of phase shift determination of resonance energies is included as well. Chapter III presents the results of our calculations. It contains figures illustrating the response functions calculated within the HF-CRPA for the neutron rich nuclei ^{60}Ca and

^{28}O and for the symmetric ^{80}Zr. We also present figures showing the Free response with a discretized continuum with different smearing parameters for ^{60}Ca and ^{28}O. The ^{60}Ca case is also shown with a different box size. We also include the outcome of the phase shift method calculations for the neutron-rich nuclei. These results are supported by a detailed discussion. In Chapter IV we present our conclusions.

CHAPTER II

FORMALISM

Hartree-Fock equations

The Hartree-Fock equations are used in general to calculate the eigenvalues and eigenstates of a many-body system. It is no surprise then that they provide the basis for nuclear collective excitations calculations such as those within the IVGDR. The discussion below regarding the HF equations is based on the material found in Ref. [4] and [5].

The essential task of any many-body problem is to solve the many-body Schrodinger equation

$$H\Psi = E\Psi, \tag{1}$$

where Ψ is the wave function for the entire system and E is its corresponding energy. In our case, one can start by constructing the many body Hamiltonian

$$H = \sum_i T_i + \frac{1}{2}\sum_{i \neq j} V_{i,j}\ , \tag{2}$$

where T_i is the kinetic energy operator for the ith particle and $V_{i,j}$ is the nuclear two-body interaction. In the simple independent particle approximation, also known as the Hartree approximation [4], [5], one writes the many-body wave function as a product of single particle wave functions,

$$\Psi = \phi_1(\boldsymbol{r_1})\phi_2(\boldsymbol{r}_2)\dots\phi_n(\boldsymbol{r}_N), \tag{3}$$

with ϕ_i representing an occupied single-particle state and $\boldsymbol{r}_i$ representing the spacial, spin and isospin coordinates of each of the N nucleons. One way to obtain an equation for the ith state would be to multiply both sides of Eq. 1 by the product of the complex conjugate remaining states and integrate over their coordinates provided that the states are chosen to be orthonormal [4]. We would obtain an equation for the ith state similar in form to the Schrodinger equation but with a potential energy term given by the average interaction energies of the remaining states. The physical interpretation is that any of the N nucleons is "moving" in a potential given by the average of all its interactions with the other particles [4]. This scheme and its interpretation are termed the mean-field approximation. More formally, one can obtain the Hartree Equations by starting with an overall wave function given by Eq. 3 and applying the variational principle to the expectation value of the system's energy, while constraining the single-particle states to be orthonormal [5]. The resulting equations are the Hartree Equations as shown below

$$\left[T_i + \sum_{k=1}^{N} \int d\boldsymbol{r}' \phi_k^*(\boldsymbol{r}') V(\boldsymbol{r}, \boldsymbol{r}') \phi_k(\boldsymbol{r}')\right] \phi_i(\boldsymbol{r}) = \epsilon_i' \phi_{\boldsymbol{i}}(\boldsymbol{r}). \tag{4}$$

The major issue with the Hartree equations is the inclusion of a self-energy term, i.e. the summation also includes the ith state, which is not physical. To circumvent this problem we could exclude the ith state from the summation, resulting in a potential formally different for each fermion, an unphysical aspect considering the mean-field approximation scheme and that the nucleons are indistinguishable [4], [5]. These

difficulties were resolved by constructing an overall antisymmetric wave function through the use of a Slater determinant

$$\Psi(\boldsymbol{r}_1, \boldsymbol{r}_2, \ldots \boldsymbol{r}_N) = \frac{1}{\sqrt{N!}} \begin{vmatrix} \phi_1(\boldsymbol{r_1}) & \phi_2(\boldsymbol{r}_2) & \ldots \\ \phi_1(\boldsymbol{r_2}) & \phi_2(\boldsymbol{r_2}) & \ldots \\ \ldots & \ldots & \ldots \end{vmatrix}. \tag{5}$$

To derive the Hartree-Fock equations, we start with an antisymmetric wave function and apply the variational principle to the expectation value of the system while constraining the single-particle states to be orthonormal through the use of Lagrange multipliers. We obtain the Hartree-Fock equations shown below

$$T_i \phi_{\boldsymbol{i}}(\boldsymbol{r}) + \sum_{k=1}^{N} \int d\boldsymbol{r}' \phi_k^*(\boldsymbol{r}') V(\boldsymbol{r}, \boldsymbol{r}') \phi_k(\boldsymbol{r}') \phi_i(\boldsymbol{r}) -$$

$$\sum_{k=1}^{N} \int d\boldsymbol{r}' \phi_k^*(\boldsymbol{r}') V(\boldsymbol{r}, \boldsymbol{r}') \phi_i(\boldsymbol{r}') \phi_k(\boldsymbol{r}) = \epsilon_i' \phi_{\boldsymbol{i}}(\boldsymbol{r}). \tag{6}$$

The presence of the second summation eliminates the self-energy problem of the Hartree equations and ensures that formally the potential is the same for all particles [4]. Note that this second term is in general non-local [4]. These equations form the basis of the HF-RPA for the IVGDR.

Green's function approach to the linear response function

We are essentially studying the response of the system under the influence of an external oscillating field. As such, we need to consider the time-dependent Hartree-Fock theory.

We start with the static Hartree-Fock equations derived above and then add a time-dependent perturbation.

We follow the derivation for the RPA Green's function given in Ref. [6]. We define the density as

$$\rho = \sum_i \phi_i^* \phi_i, \tag{7}$$

such that the Hartree-Fock equations can be written as

$$H[\rho]\phi_i = \epsilon_i \phi_i. \tag{8}$$

We introduce an external field to H in the form of

$$e^{-i\omega t} V_{ext}(r) + H.C., \tag{9}$$

which produces a density oscillation of the form

$$\rho = \rho_0 + \left(\rho' e^{-i\omega t} + H.C.\right), \tag{10}$$

where ρ_0 is the unperturbed density and

$$\rho' = \sum_{occupied} \left(\phi_i' \phi_i^{0*} + \phi_i^{*\prime} \phi_i^0\right). \tag{11}$$

The single-particle wave functions must be of the form

$$\phi_i = \phi_i^0 + e^{-i\omega t}\phi_i' + e^{i\omega t}\phi_i'', \tag{12}$$

such that ϕ_i', ϕ_i'' are orthogonal to ϕ_i^0. The time-dependent Hartree-Fock equations are written as

$$\left\{H_0 + \left(e^{-i\omega t} V_{ext} + e^{-i\omega t}\frac{\delta V}{\delta \rho}\rho' + H.C.\right) - \epsilon_i\right\}\phi_i = i\frac{d}{dt}\phi_i, \tag{13}$$

where H_0 is the unperturbed Hartree-Fock Hamiltonian. Based on the above considerations we can construct a bare Green's function as

$$G^{(0)}(r_1, r_2, \omega) = -\sum_i \phi_i^0(r_1)\left[\frac{1}{H_0 - \epsilon_i - \omega} + \frac{1}{H_0 - \epsilon_i + \omega}\right]\phi_i^0(r_2). \quad (14)$$

To obtain a computable form, we expand

$$\frac{1}{H_0 - E_i - \omega} = \sum_m \phi_m^{0*}(r_1)\frac{1}{\epsilon_m - \epsilon_i - \omega}\phi_m^0(r_2) \quad (15)$$

in terms of the Hartree-Fock unperturbed states. As such the bare Green's Function is

$$G^{(0)}(r_1, r_2, \omega) = -\sum_{i,m} \phi_i^{0*}(r_1)\phi_m^0(r_1)\left[\frac{1}{\epsilon_m - \epsilon_i - \omega} + \frac{1}{\epsilon_m - \epsilon_i + \omega}\right]\phi_m^{0*}(r_2)\phi_i^0(r_2). \quad (16)$$

The RPA Green's Function is given by

$$G^{RPA} = G^{(0)}\left(1 + \frac{\delta V}{\delta \rho}G^{(0)}\right)^{-1}. \quad (17)$$

The Green's function contains all the information regarding our system and thus relevant properties can be extracted from it. The transition strength out of the system ground state induced by a field f [6] is

$$\sum_n |\langle n|f|0\rangle|^2 \delta(E - E_n) = \frac{1}{\pi}\int d\boldsymbol{r} d\boldsymbol{r}' f^*(\boldsymbol{r}) ImG(\boldsymbol{r}, \boldsymbol{r}', E) f(\boldsymbol{r}'). \quad (18)$$

Discretized vs. continuum treatment

In our calculations, the operator equations defining the bare and RPA Green's functions are rewritten as matrix equations on a mesh in coordinate space [7]. If the unperturbed Hartree-Fock Hamiltonian H_0 has a discrete spectrum as is the case when the continuum is discretized, the single-particle Green's function [7] is given by

$$\left(\frac{1}{H_0 - E}\right)_{r_1 r_2} = \sum_m \phi_m^{0*}(r_1)\frac{1}{\epsilon_m - E}\phi_m^0(r_2). \tag{19}$$

The exact treatment of the continuum can be undertaken by writing the single-particle Green's function [7] as

$$g_{lj}(r_1, r_2, E) = \frac{1}{H_0 - E} = -\frac{\frac{2m}{\hbar^2}u_{lj}(r_<)v_{lj}(r_>)}{W}, \tag{20}$$

where W is the Wronskian ensuring the proper normalization of the Green's function

$$W = u\frac{dv}{dr} - v\frac{du}{dr}. \tag{21}$$

In the expression for the single-particle Green's function u_{lj} is the regular solution to the Hartree-Fock Hamiltonian for the lj partial wave, and v_{lj} is the irregular solution which is determined by the boundary condition at infinity while $r_<$ and $r_>$ denote the lesser and the greater of r_1 and r_2 respectively [7]. We thus have [7]

$$v_{lj} \sim \exp\left(-\sqrt{\frac{2m|E|}{\hbar^2}}r\right), \qquad r \to \infty \text{ and } E \leq 0 \tag{22}$$

, and

$$v_{lj} \sim \exp\left(i\sqrt{\frac{2mE}{\hbar^2}}r\right), \qquad r \to \infty \text{ and } E > 0. \tag{23}$$

The response of the system is determined by Eq. 18 using the form of the Green's Function given by Eq. 14, 17 and 20.

Phase shift calculations

A single-particle resonance is defined by an increasing phase shift going through π/2 corresponding to peaks in the derivatives of the phase shifts of the single-particle states. The derivative of the single-particle phase shift is related to the single-particle level density. To check the results of our HF-CRPA calculations we carry out calculations of the derivatives of the single-particle phase shifts using both the method of phase shift and Green's function. In the latter approach, the density is calculated by subtracting the Green's function of a free Hamiltonian from the Green's function associated with a Hamiltonian including interactions.

Phase shift method

To determine the single-particle level density we put the system in a large spherical box of radius R and consider the asymptotic behavior of the regular solution [8]

$$\lim_{r\to\infty}\psi_l = const\frac{1}{r}\sin(kr-\frac{1}{2}l\pi+\delta_l(\epsilon)), \qquad \epsilon>0\,, \tag{24}$$

where $k=\sqrt{2m\varepsilon/\hbar^2}$ is the wave number and $\delta_l(\varepsilon)$ is the phase shift for a finite range potential which vanishes at infinity faster than $1/r$. The condition for finite wave functions is to set $\psi_l(R)=0$ such that

$$kR-\frac{1}{2}l\pi+\delta_l(\epsilon)=s\pi, \tag{25}$$

s being an integer. The single-particle level density [8] is then given by

$$g_{Cl}^{tot}(\epsilon)=2(2l+1)\frac{ds}{d\epsilon}=\frac{1}{\pi}2(2l+1)\frac{d\delta_l(\epsilon)}{d\epsilon}+\frac{2(2l+1)}{\pi}R\frac{dk}{d\epsilon}, \tag{26}$$

where the second term is the free-gas contribution. By subtracting it from the expression above [8] we obtain the single-particle level density in the continuum

$$g_{Cl}(\epsilon) = \frac{1}{\pi} 2(2l+1) \frac{d\delta_l(\epsilon)}{d\epsilon}. \quad (27)$$

Near a resonant energy [8]

$$\frac{d\delta_l(\epsilon)}{d\epsilon} = \frac{\Gamma_{R/2}}{(\epsilon_R - \epsilon)^2 + (\frac{\Gamma_R}{2})^2} \approx \pi\delta(\epsilon - \epsilon_R), \ \Gamma_R \to 0. \quad (28)$$

As a consequence of Levinson's theorem [8] the phase shifts at zero energy, $\delta_l(0)$, and infinity , $\delta_l(\infty)$, are related to the number of bound states, N_l, by

$$\delta(0) - \delta(\infty) = N_l \pi. \quad (29)$$

Green's function

The single-particle level density can also be calculated using Green's function [8]. The single-particle level density is given by

$$g_l(\epsilon) = \lim_{\alpha\to\infty, R\to\infty} 2(2l+1)\frac{1}{\pi}\int_0^R dr[\mathrm{Im}G_l(r,r',\epsilon+i\alpha) - \mathrm{Im}G_{0l}(r,r',\epsilon+i\alpha)]_{r=r'}, \quad (30)$$

where G_{0l} is associated with the free Hamiltonian. For the exact treatment of the continuum we used the expression developed above for this purpose.

CHAPTER III

RESULTS

We will successively present the HF-CRPA results, the Free response with a discretized continuum results and the phase shift results. For convenience, both HF-CRPA and discretized responses have been normalized by integrating up to 40 MeV. All calculations ignore Coulomb interactions while the discretized calculations specifically ignore symmetry energy. The HF single-particle energies are important and will be referenced throughout the discussion. These are shown in Table I.

HF-CRPA results

We are interested in the low energy enhancements appearing in the RPA response for the asymmetric nuclei ^{60}Ca and ^{28}O. We show the RPA response of ^{60}Ca and ^{28}O for dipole transitions in Figs.1 and 2 respectively. To illustrate the neutron threshold effect for dipole excitations in neutron-rich nuclei we also present the RPA response for ^{80}Zr, a nucleus with equal number of protons and neutrons, in Fig. 3. These RPA responses were calculated within the HF-CRPA scheme described in the formalism using a maximum radius of 12 fm. The results include a smearing of 0.4 MeV and are plotted as functions of excitation energies. The RPA responses are shown in the top sides of the figures while the bottom sides show the real part of $\langle fGf \rangle$. We notice prominent enhancements in the

RPA response in the 10-15 MeV range for all three nuclei. Our main point of interest however lies in the relatively weaker enhancements present in the 5-7.5 MeV range for ^{60}Ca and ^{28}O. To calculate the response of the system under the RPA we use nuclear wave functions which are linear combinations of Slater determinants corresponding to different possible nuclear configurations for single-particle dipole transitions. To understand the origin of the low energy enhancements in the RPA responses and determine whether these can be interpreted as resonances we need to analyze the Free responses of the systems which show the strengths and positions of single-particle excitations.

The Free response is given by the imaginary part of $\langle fG^{(0)}f\rangle$. For transitions below threshold, $\langle fG^{(0)}f\rangle$ has no imaginary part while the real part has poles. The use of the finite smearing allows us to numerically determine the positions and strengths of these transitions while giving them a "nominal" fixed width. In the HF-CRPA scheme, for transitions to the continuum, the particle states are free to decay and the widths of these states are properly included. For resonances, these widths are very small and the imaginary part of $\langle fG^{(0)}f\rangle$ i.e. Free response, will have the characteristic Breit-Wigner resonance shape while the real part will have a pole.

The Free responses for ^{60}Ca, ^{28}O and ^{80}Zr under the HF-CRPA scheme for a maximal radius of size 12 fm are shown in Figs. 4, 5 and 6 respectively. In each figure, the top contains the imaginary part of $\langle fG^{(0)}f\rangle$, while the bottom illustrates the real part of

$\langle fG^{(0)}f\rangle$. The results contain a smearing of Γ/2=0.4 MeV and are plotted as functions of excitation energy.

TABLE I. Single-Particle Orbits calculated from the HF equations. The broad lines indicate the last occupied state.

HF Single-Particle Energies (MeV)

	^{28}O		^{60}Ca		^{80}Zr	
Orbits	Proton	Neutron	Proton	Neutron	Proton	Neutron
0s1/2	-26.824	-26.824	-29.919	-29.919	-30.792	-30.792
0p3/2	-17.882	-17.882	-23.776	-23.776	-25.569	-25.569
0p1/2	-17.882	-17.882	-23.776	-23.776	-25.569	-25.569
0d5/2	-7.614	-7.614	-16.350	-16.350	-19.139	-19.139
0d3/2	-7.614	-7.614	-16.350	-16.350	-19.139	-19.139
1s1/2	-5.225	-5.225	-13.591	-13.591	-16.438	-16.438
0f7/2			-7.952	-7.952	-11.714	-11.714
0f5/2			-7.952	-7.952	-11.714	-11.714
1p3/2			-4.674	-4.674	-7.998	-7.998
1p1/2			-4.674	-4.674	-7.998	-7.998
0g9/2					-3.536	-3.536
0g7/2					-3.536	-3.536
1d5/2					-0.255	-0.255
1d3/2					-0.255	-0.255
2s1/2					-0.255	-0.255

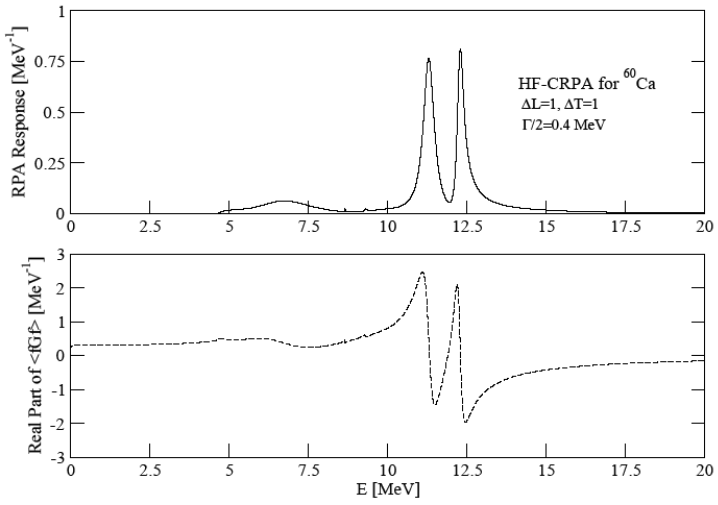

FIG. 1. Isovector Dipole Continuum HF-CRPA for ^{60}Ca with smearing Γ/2=0.4 MeV and a maximum radius of 12 fm. The imaginary part of $\langle fGf \rangle$ (RPA response) is shown on top while the real part of $\langle fGf \rangle$ is shown on the bottom. To better distinguish between the two, the real part of $\langle fGf \rangle$ is dashed.

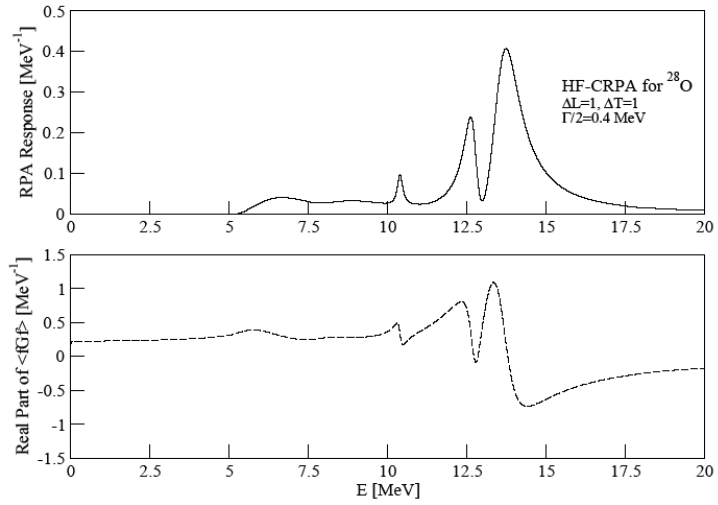

FIG. 2. Isovector Dipole Continuum HF-CRPA for ^{28}O with smearing Γ/2=0.4 MeV and a maximum radius of 12 fm. The imaginary part of $\langle fGf \rangle$ (RPA response) is shown on top while the real part of $\langle fGf \rangle$ is shown on the bottom. To better distinguish between the two, the real part of $\langle fGf \rangle$ is dashed.

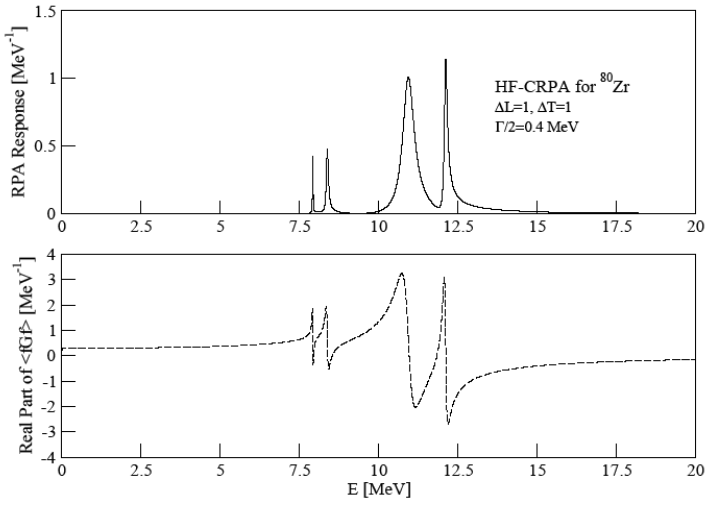

FIG. 3. Isovector Dipole Continuum HF-CRPA for ^{80}Zr with smearing Γ/2=0.4 MeV and a maximum radius of 12 fm. The imaginary part of $\langle fGf \rangle$ (RPA response) is shown on top while the real part of $\langle fGf \rangle$ is shown on the bottom. To better distinguish between the two, the real part of $\langle fGf \rangle$ is dashed.

We now turn to analyze the Free response for ^{60}Ca shown in Fig. 4. The strong transitions at 8.50, 8.92 and 11.68 MeV correspond to the proton dipole bound-to-bound excitations $\pi 0d \rightarrow \pi 0f$, $\pi 1s \rightarrow \pi 1p$ and $\pi 0d \rightarrow \pi 1p$ respectively. For these, we notice that the real part of $\langle fG^{(0)}f \rangle$ goes through zero as discussed above. These peaks were identified using the HF single-particle energies shown in Table I. Our main point of interest rests with the enhancements in the Free response in the 5-7.5 MeV excitation energy range. While we do see an enhancement in the Free response, the real part of $\langle fG^{(0)}f \rangle$ does not show any poles in this region. We can say then that these enhancements are not resonances but are due to neutron transitions to the continuum. The excitations in this range contribute the

most to the low-energy enhancement in the RPA response discussed above. Since we determined that the 5-7.5 MeV transitions are not single-particle resonances in the Free response, the enhancement seen in the RPA in the 5-7.5 MeV range is most likely not a low-energy resonance but is related to the neutron single-particle transitions to the continuum.

The same arguments apply in the case of ^{28}O. The strong transitions at 10.27 and 12.66 MeV in the Free response of ^{28}O shown in Fig. 5 are the proton bound-to-bound transitions $\pi 0p \rightarrow \pi 0d$ and $\pi 0p \rightarrow \pi 1s$ respectively. The HF states for this nucleus can also be seen in Table I. The enhancement seen in the RPA response for ^{28}O in the 5-7.5 MeV range can be linked to the non-resonance single-particle neutron transitions to the continuum which give rise to the enhancement in the Free response in the same energetic region for this nucleus.

The Free response for ^{80}Zr is shown in Fig. 6. These calculations used a maximum radius of 12 fm. We can identify the peaks at 7.74, 8.18 and 11.46 MeV as either proton or neutron bound-to-bound transitions $1p \rightarrow 1d$ and $1p \rightarrow 2s$ for the first peak, $0f \rightarrow 0g$ for the second and $0f \rightarrow 1d$ for the last peak. We note the absence of enhancements in the Free response in the 5-7.5 MeV range due to the threshold energy of 7.998 MeV for both protons and neutrons. Small enhancements in the Free response can be seen at energies higher than the threshold. The contribution of these peaks to the RPA response shown in Fig. 3 is almost completely obscured by the giant resonances at roughly 8 and 11 MeV.

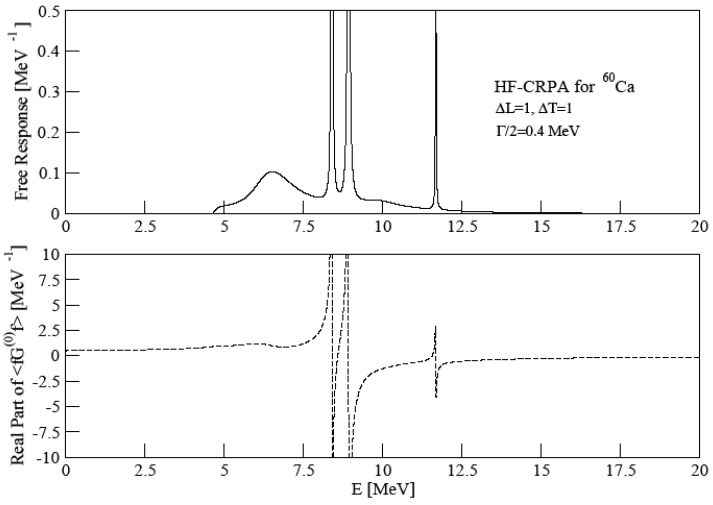

FIG. 4. Isovector Dipole Continuum HF-CRPA Free Response for ^{60}Ca with smearing Γ/2=0.4 MeV and a maximum radius of 12 fm. The imaginary part of $\langle fG^{(0)}f\rangle$ (Free response) is shown on top while the real part of $\langle fG^{(0)}f\rangle$ is shown on the bottom. To better distinguish between the two, the real part of $\langle fG^{(0)}f\rangle$ is dashed.

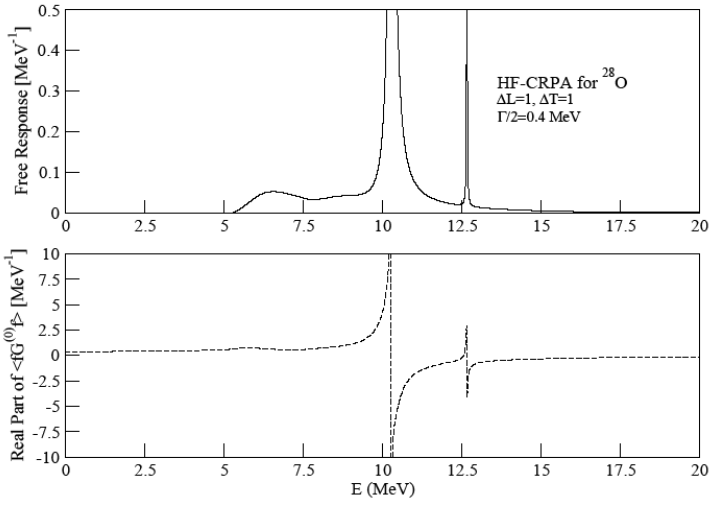

FIG. 5. Isovector Dipole Continuum HF-CRPA Free response for ^{28}O with smearing Γ/2=0.4 MeV and a maximum radius of 12 fm. The imaginary part of $\langle fG^{(0)}f\rangle$ (Free response) is shown on top while the real part of $\langle fG^{(0)}f\rangle$ is shown on the bottom. To better distinguish between the two, the real part of $\langle fG^{(0)}f\rangle$ is dashed.

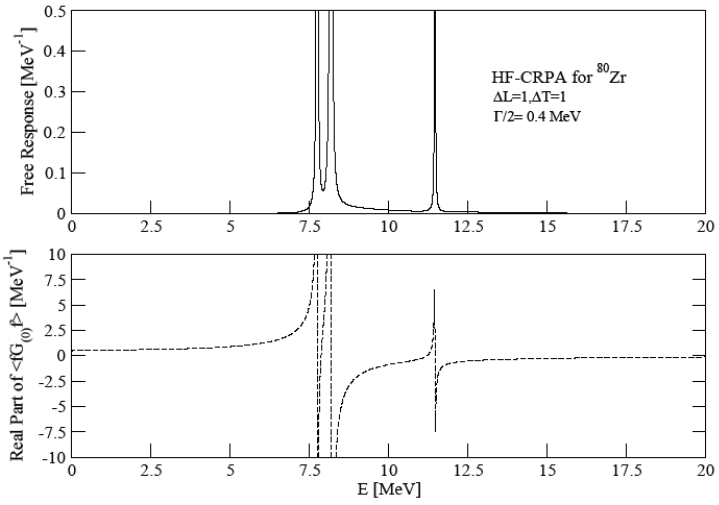

FIG. 6. Isovector Dipole Continuum HF-CRPA Free response for ^{80}Zr with smearing Γ/2=0.4 MeV and a maximum radius of 12 fm. The imaginary part of $\langle fG^{(0)}f\rangle$ (Free response) is shown on top while the real part of $\langle fG^{(0)}f\rangle$ is shown on the bottom. To better distinguish between the two, the real part of $\langle fG^{(0)}f\rangle$ is dashed.

Free response with a discretized continuum

In a typical HF-DRPA scheme, the continuum is discretized. This is done in practice by the use of a spherical box. The latter ensures that the single-particle continuum states are in fact still bound states of positive energy. In turn, all single-particle transitions to the continuum are treated in the same manner as bound-to-bound transitions. Referring to the discussion above, single-particle bound-to-bound transitions are given a fixed width through smearing. Thus, all transitions to the continuum will also have the same width as bound-to-bound transitions. Their contribution to the RPA could give rise to low energy

enhancements which could be incorrectly interpreted as resonances in the collective response. Smearing with large parameters contributes to this effect. In addition, the size of the box is also an important parameter which will be discussed below. As we have seen above, our HF-CRPA calculations indicate that the low energy enhancements in the RPA responses are not resonances.

To show how this could come about we present the isovector dipole Free response for ^{60}Ca with a discretized continuum with a box of 150 fm in Fig. 7. The top side of the figure shows the Free response with a smearing of $\Gamma/2$=0.04 MeV while the bottom shows the same calculations with a smearing of 0.4 MeV. In the top section, we recognize the peaks at 8.4, 8.9 and 11.68 MeV as the proton bound-to-bound transitions discussed above.

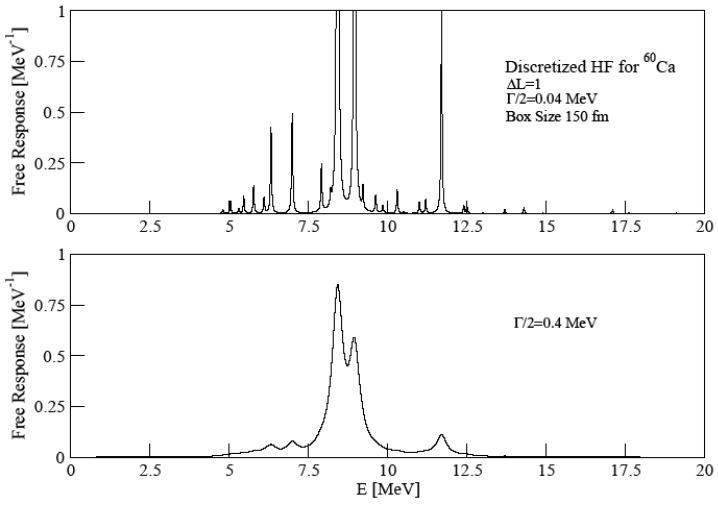

FIG. 7. Isovector Dipole Discretized HF for ^{60}Ca with a box size of 150 fm. The top part shows the Free response with smearing Γ/2=0.04 MeV while the bottom shows the Free response with smearing Γ/2=0.4 MeV.

We also see that the peaks in the 5-7.5 MeV range are neutron transitions to the continuum. Despite their relative weakness, these transitions to the continuum are given the same width as the strong bound-to-bound transitions through smearing. We notice that the enhancement seen in the HF-CRPA Free response shown in the top of Fig. 4 in the 5-7.5 MeV range is distributed among isolated peaks due to the discretization of the continuum as seen in Fig. 7. Qualitatively, the strength of these discrete peaks follows the shape of the enhancement seen in the same range for the HF-CRPA calculations. The bottom of Fig. 7 illustrates the effect of larger smearing. We see that for a smearing of Γ/2=0.4 MeV the discretized results have a form similar to the HF-CRPA results. We

emphasize again, that our HF-CRPA results indicate that there are no resonances in the 5-7.5 MeV region and we are strongly inclined to say the same for the discretized results.

The Free response for ^{28}O with a discretized continuum and a box of 150 fm is shown in Fig. 8. It can be qualitatively interpreted as discussed above.

To show the effect of the box size on the single-particle transition strengths, we present the Free response for ^{60}Ca with a discretized continuum with a box size of 12 fm in Fig. 9. The top and bottom again correspond to $\Gamma/2$=0.04 MeV and $\Gamma/2$=0.4 MeV respectively. Instead of the multitude of transitions in the 5-7.5 MeV range and elsewhere we only notice two strong peaks in the alluded region. Because of the distinct presence of these strong peaks one is easily inclined to interpret them as single-particle resonances. In light of what has been said, it is clear that they are not resonances.

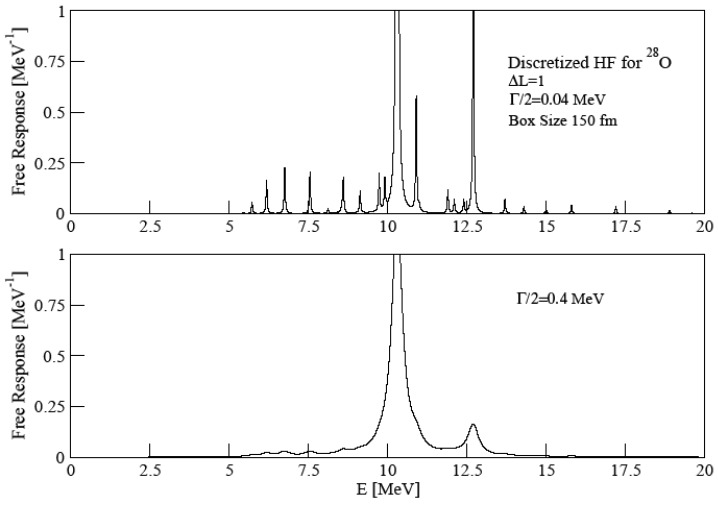

FIG. 8. Isovector Dipole Discretized HF for ^{28}O with a box size of 150 fm. The top part shows the Free response with smearing Γ/2=0.04 MeV while the bottom shows the Free response with smearing Γ/2=0.4 MeV.

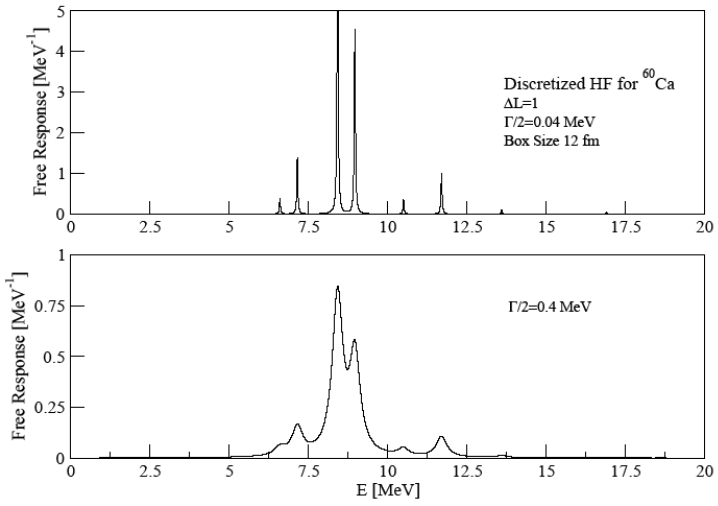

FIG. 9. Isovector Dipole Discretized HF for ^{60}Ca with a box size of 12 fm. The top part shows the Free response with smearing Γ/2=0.04 MeV while the bottom shows the Free response with smearing Γ/2=0.4 MeV.

Phase shift results

To confirm our HF-CRPA results we calculated the derivatives of the scattering phase shifts for ^{60}Ca and ^{28}O with no Coulomb interactions and with a mean-field potential determined from the HF-CRPA. The phase shift calculations were also done by both the phase shift method properly and the Green's function method as described in the formalism. In practice, this was achieved using an existing program that calculated the single-particle level densities. We focus on calculations in the continuum. As Eq. 27 shows, for a fixed angular momentum, the derivative of the scattering phase shift is proportional to the single-particle level density in the continuum. In addition, the single-particle level density can also be calculated using Green's function as illustrated in Eq.30. It is important to clarify that the object of interest was the calculation of the derivatives of the scattering phase shifts and not the single-particle densities.

In Fig. 10 we present the results of the phase shift derivative calculations for L=4 for ^{60}Ca. Starting from the top we list the integral of the imaginary part of the Green function with interactions, the integral of the imaginary part of the Green's function associated with the free Hamiltonian and the difference between the two integrals which ,according to Eq.30, is proportional to the phase shift derivative. The results shown at the bottom calculated according to the phase shift method are proportional to the scattering phase shift as well. All are plotted as functions of state energy, not excitation energy. Note that the Green's function results contain a smearing of Γ=0.8 MeV.

The L=0, 1, 2, 3 and 5 cases are shown in Figs. A1, A2, A3, A4 and A5 in the Appendix. For negative energies, the states are discretized. Referring to the very bottom of the figures, we note that there are no enhancements for negative energies in the phase shift densities since no calculations were undertaken in this region with the method characterized by Eq. 24-27. For the L=0 and L=1 cases we see that the densities of states in the continuum calculated from both the Green's function and the phase shift method show pronounced drops to negative values with long tails extending to infinity. This behavior can be justified by a consequence of Levinson's theorem, as described by Eq.29. In the L=2 case we notice peak-like enhancements immediately after zero energy for both Green's function and phase shift calculations. We emphasize that the sharp increases in the densities right after zero are in fact related to the specific numerical details of the calculations and do not correspond to gradual increases in the scattering derivatives. For states of L=3 to L=5 we see actual positive peaks occurring in the continuum single-particle densities. After each peak, one also notices a drop below zero in the density. This again can be explained by Levinson's theorem.

It is important to note that only the L=4 and L=5 peaks are in fact resonances. This is because at the resonant energy the phase shift has to go through $\pi/2$. For the L=3 peak the phase shift at the energy corresponding to the maxima in the density peak is much lower than $\pi/2$. The only resonances therefore occur for L=4 and L=5.

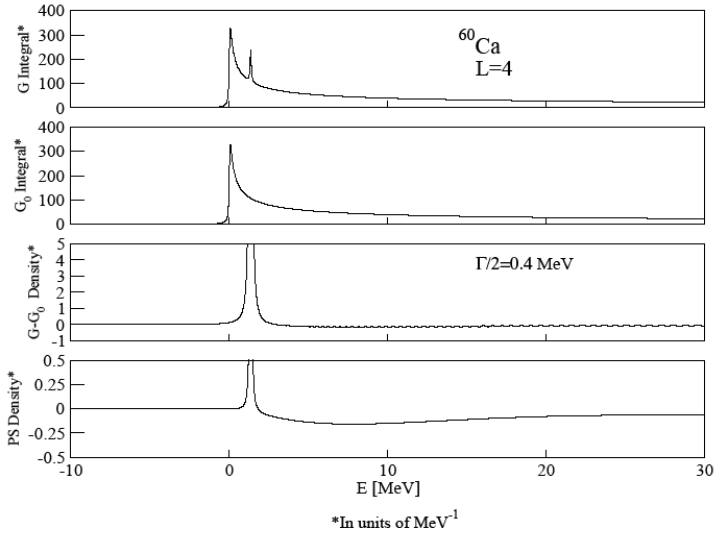

FIG. 10. Single-Particle Level Density for ^{60}Ca, for L=4. The results are plotted as functions of state energy. A resonance at 1.36 MeV is found. A smearing of Γ/2=0.4 MeV was used in the Green's function calculations.

If the neutron transitions to the continuum as seen in the HF-DRPA were indeed resonances we should also see resonances in the phase shift derivative at the same energies for the states in the continuum. Table I gives the singe-particle energies for our nuclei. For the isovector dipole in ^{60}Ca, only the neutrons in the bound 0f state can transition to a single-particle state in the continuum of L=4. For this particular angular momentum, the sharp resonance in the density occurs at about 1.36 MeV and it would correspond to a transition from a bound neutron state of energy -7.952 MeV putting the excitation energy at about 9.312 MeV, much higher than our region of interest. No dipole transitions to an L=5 state are possible for this nucleus. We can thus conclude that

the low-energy single-particle transitions to the continuum are not resonances, in accordance with the HF-CRPA results.

We also carried out phase shift calculations for ^{28}O for L=0-5. Out of the six possibilities only the L=3, 4 and 5 cases present resonances. For L=3 this can be seen in Fig. 11 which shows the phase shift results for this nucleus with a smearing of Γ=0.8 MeV for the Green's function results. The L=0,1,2,4 and 5 cases are shown in Figs. A6, A7, A8, A9 and A10 in the Appendix. Note that the L=1 apparent enhancement beyond zero energy is not a genuine peak.

The resonance for L=3 occurs at approximately 3.38 MeV in state energy. Table I indicates that for an excited state in the continuum of L=3 only the 0d bound neutron can transition. This would require an excitation energy of 11 MeV which, as in the case of ^{60}Ca, is much higher than the 5-7.5 MeV region of interest. Dipole transitions to states of L > 3 are not possible. This confirms our HF-CRPA results which indicated that ^{28}O did not have resonances in the Free response in the 5-7.5 MeV range.

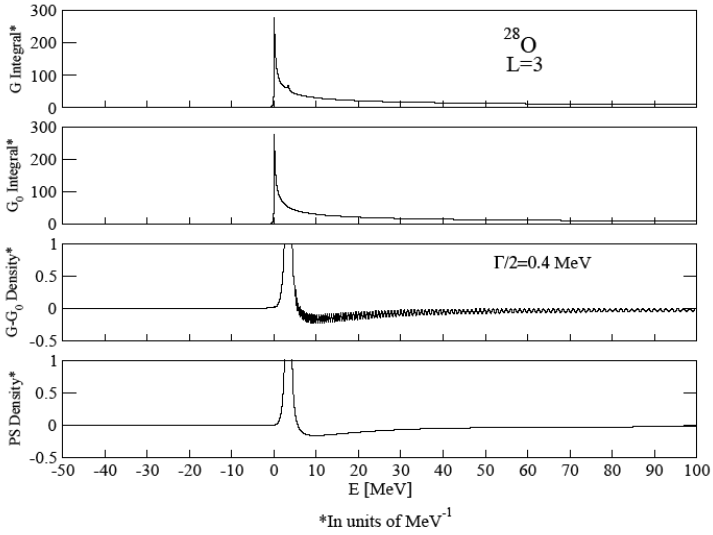

FIG. 11. Single-Particle Level Density for ^{28}O, for L=3. The results are plotted as functions of state energy. A resonance at 3.38 MeV is found. A smearing of Γ/2=0.4 MeV was used in the Green's function calculations.

CHAPTER IV

CONCLUSION

We carried out HF-CRPA calculations for the two asymmetric nuclei ^{60}Ca and ^{28}O and the symmetric nucleus ^{80}Zr. In the case of the asymmetric nuclei, we found low energy enhancements in the RPA response. To investigate these enhancements in the collective spectrum of the asymmetric nuclei, we determined the Free response for the latter which illustrated the particle-hole transition strengths. In particular, we analyzed the enhancement in the Free response in the 5-7.5 MeV range. Upon detailed consideration of the HF-CRPA results, we determined that the enhancements in the Free responses in this range were due entirely to neutron non-resonance transitions to the continuum.

In the literature, it is common to undertake HF-RPA calculations with a continuum discretized by the use of a spherical box. To illustrate some of the issues with this approach, we determined the Free response for ^{60}Ca and ^{28}O with a discretized continuum. This method uses discrete continuum states with all single-particle transitions, either bound-to-bound or to the continuum, being given the same width through smearing. Non-resonance transitions to the continuum are thus likely to be interpreted as resonances in the Free response. To show this, we compared the results of the discretized calculations with those undertaken with the proper treatment of the continuum. It was shown that the smooth enhancement in the Free HF-CRPA response in the 5-7.5 MeV range was distributed among narrow discrete peaks in the Free HF-

DRPA response. The increase in the size of the spherical box for the HF-DRPA resulted in the strength of the Free response being distributed among an increasing number of discrete peaks. We also showed that the HF-CRPA and HF-DRPA Free responses have similar shapes with increasing smearing.

Our HF-CRPA results were confirmed by the phase shift calculations for ^{60}Ca and ^{28}O. We showed that resonances in the derivatives of the scattering phase shifts implied single-particle excitations of energies much higher than our 5-7.5 MeV region of interest.

In conclusion, we have established that the enhancements in the Free responses of the two asymmetric nuclei in the excitation energy range of 5-7.5 MeV are due to non-resonance neutron transitions to the continuum and that these transitions only appear as resonances in discretized calculations. These sharp transitions are spurious and are a direct consequence of the discretization of the continuum. As such, low energy enhancements in the RPA responses of these nuclei with a discretized continuum are not resonances.

REFERENCES

[1] G.C. Baldwin and G.S. Klaiber, Phys. Rev. **71**, 3 (1947)

[2] M. Goldhaber and E. Teller, Phys. Rev. **74**, 1046 (1948)

[3] H. Steinwedel, J. H. Jensen, and P. Jensen, Phys. Rev. **79**, 1019 (1950)

[4] J. Thijssen, *Computational Physics* (Cambridge, New York, 2007), 2nd Ed., Chap.4

[5] A. Messiah, *Quantum Mechanics* (Dover, Mineola, New York, 1999), Vol.2, Chap.18

[6] G. F. Bertsch and S. F. Tsai, Phys. Rep. **18**, 125 (1975)

[7] S. Shlomo and G. Bertsch, Nucl. Phys. **A243**, 507 (1975)

[8] S. Shlomo, V.M. Kolomietz, and H. Dejbakhsh, Phys. Rev. C **55**, 1972 (1997)

APPENDIX

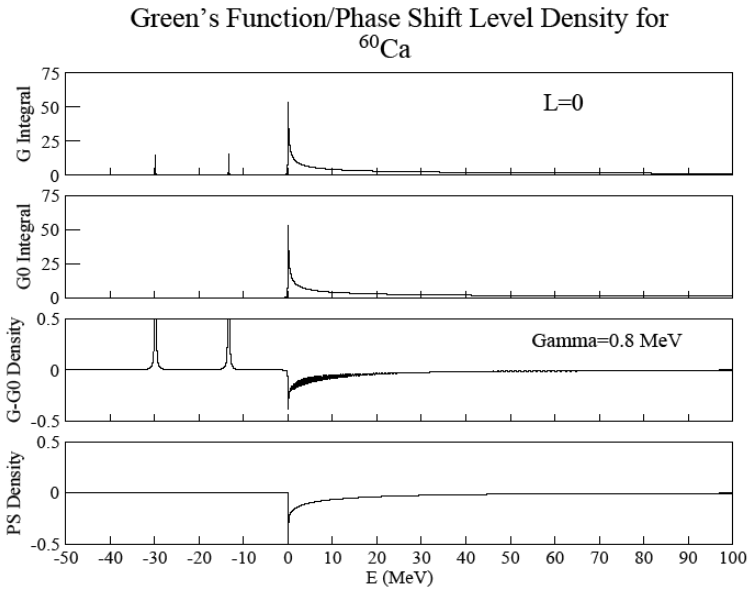

FIG. A1. Single-Particle Level Density for ^{60}Ca for L=0 with $\Gamma/2$=0.8 MeV.

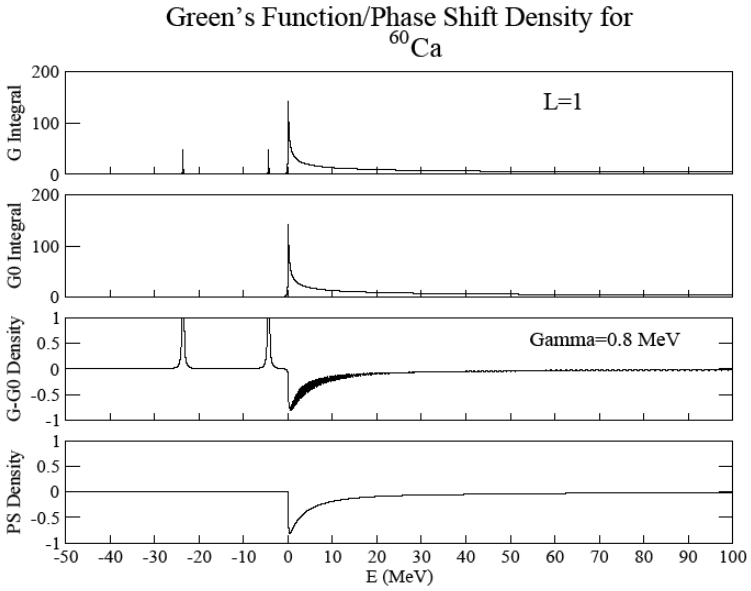

FIG. A2. Single-Particle Level Density for ^{60}Ca for L=1 with $\Gamma/2$=0.8 MeV.

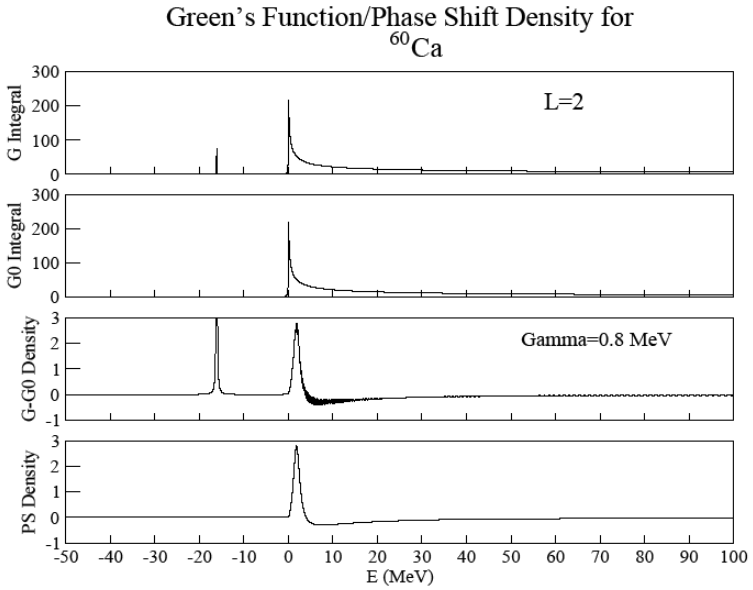

FIG. A3. Single-Particle Level Density for ^{60}Ca for L=2 with $\Gamma/2$=0.8 MeV.

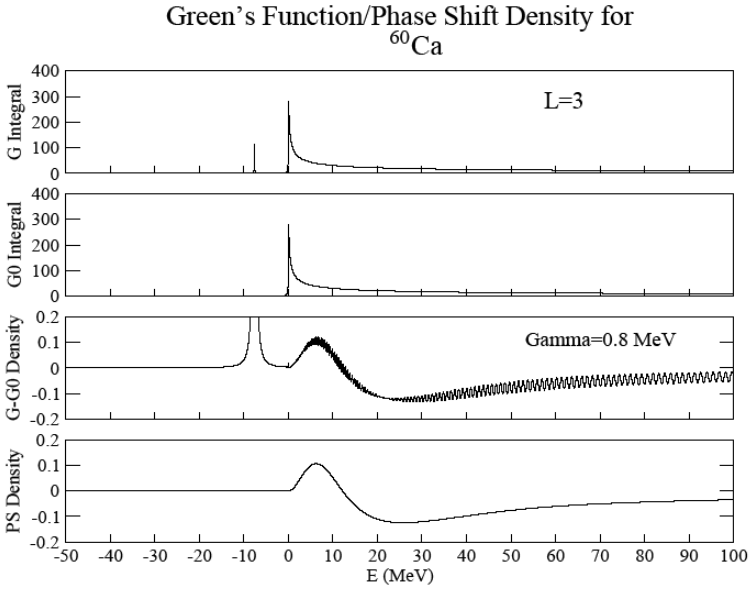

FIG. A4. Single-Particle Level Density for ^{60}Ca for L=3 with $\Gamma/2$=0.8 MeV.

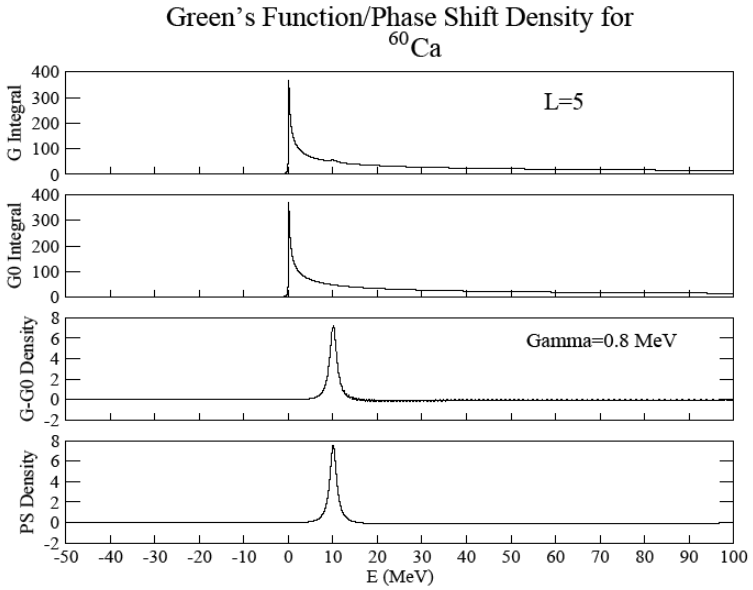

FIG. A5. Single-Particle Level Density for ^{60}Ca for L=5 with $\Gamma/2$=0.8 MeV.

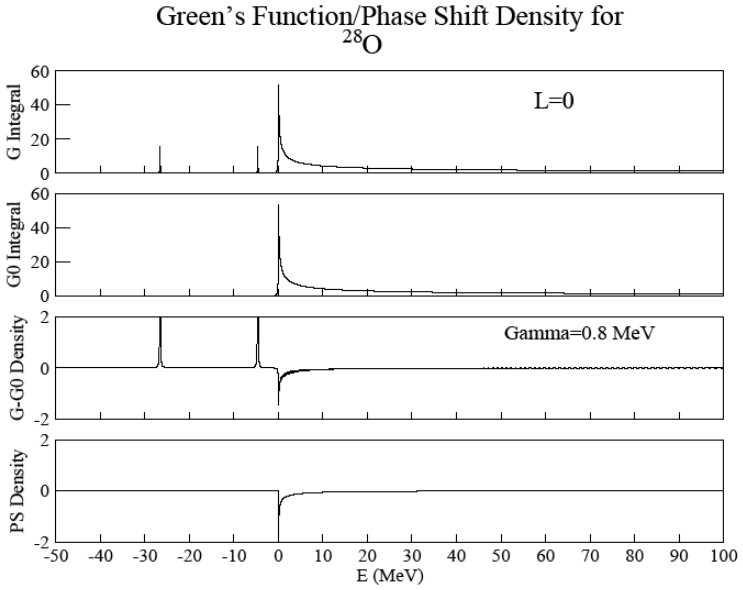

FIG. A6. Single-Particle Level Density for ^{28}O for L=0 with $\Gamma/2$=0.8 MeV.

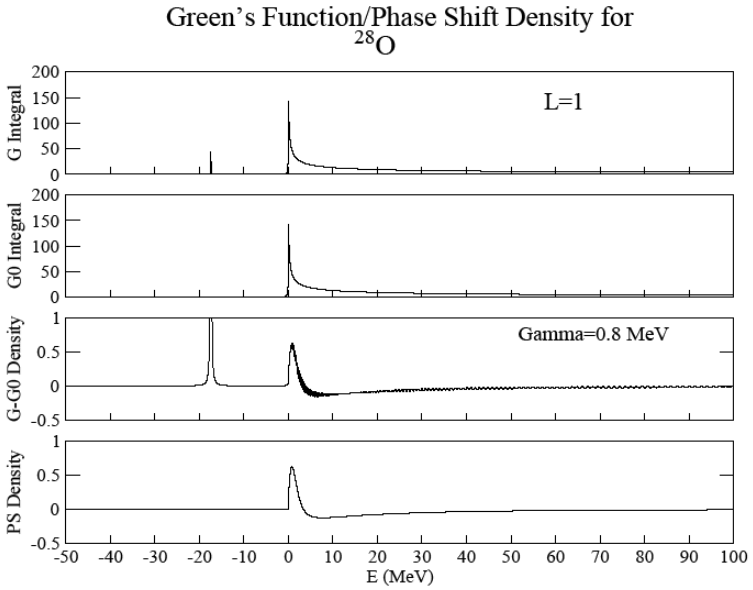

FIG. A7 Single-Particle Level Density for ^{28}O for L=1 with Γ/2=0.8 MeV.

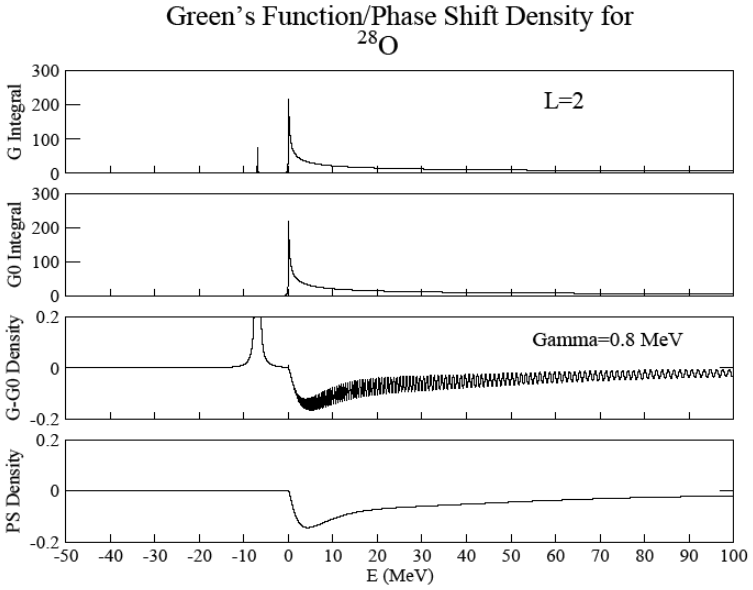

FIG. A8. Single-Particle Level Density for ^{28}O for L=2 with Γ/2=0.8 MeV.

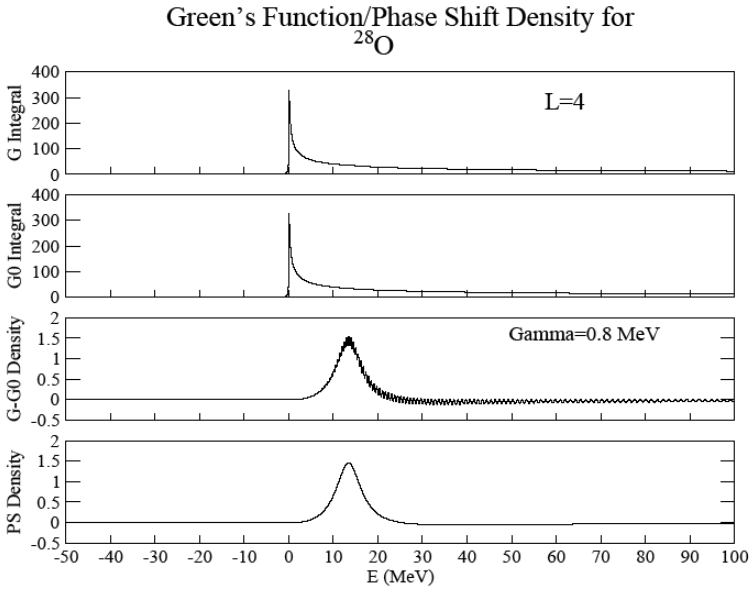

FIG. A9. Single-Particle Level Density for ^{28}O for L=4 with Γ/2=0.8 MeV

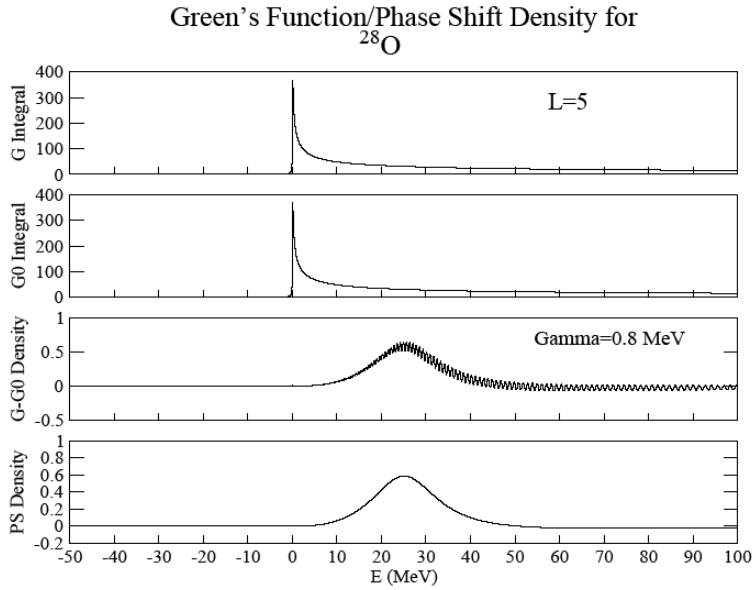

.

FIG. A10. Single-Particle Level Density for ^{28}O for L=5 with Γ/2=0.8 MeV.

CONTACT INFORMATION

Name:	Emilian Nica
Professional Address:	c/o Dr. Shalom Shlomo Cyclotron Institute Texas A&M University MS #3366 College Station TX 77843-3366
Email Address:	enica@neo.tamu.edu
Education:	B.S., Physics, Texas A&M University, August 2009 Undergraduate Research Scholar